Fermilab

Constraints on primordial non-Gaussianity from the cross-correlation of DESI Luminous Red Galaxies and Planck CMB lensing

FERMILAB-PUB-24-0942-PPD

arXiv:2412.10279

Astronomy & Astrophysics manuscript no. aanda
December 16, 2024

Constraints on primordial non-Gaussianity from the cross-correlation of DESI Luminous Red Galaxies and *Planck* CMB lensing

J. R. Bermejo-Climent[1,2⋆], R. Demina[1], A. Krolewski[3,4,5], E. Chaussidon[6], M. Rezaie[7], S. Ahlen[8], S. Bailey[6], D. Bianchi[9], D. Brooks[10], E. Burtin[11], T. Claybaugh[6], A. de la Macorra[12], Arjun Dey[13], P. Doel[10], G. Farren[6], S. Ferraro[6,14], J. E. Forero-Romero[15,16], E. Gaztañaga[17,18,19], S. Gontcho A Gontcho[6], G. Gutierrez[20], C. Hahn[21], K. Honscheid[22,23,24], C. Howlett[25], R. Kehoe[26], D. Kirkby[27], T. Kisner[6], M. Landriau[6], L. Le Guillou[28], M. E. Levi[6], M. Manera[29,30], A. Meisner[13], R. Miquel[31,30], J. Moustakas[32], J. A. Newman[33], G. Niz[34,35], N. Palanque-Delabrouille[11,6], W. J. Percival[3,4,5], F. Prada[36], I. Pérez-Ràfols[37], D. Rabinowitz[38], A. J. Ross[22,39,24], G. Rossi[40], E. Sanchez[41], D. Schlegel[6], D. Sprayberry[13], G. Tarlé[42], B. A. Weaver[13], M. White[43,14], C. Yèche[11], and P. Zarrouk[28],

(Affiliations can be found after the references)

Received XXX; accepted YYY

ABSTRACT

Aims. We use the angular cross-correlation between a Luminous Red Galaxy (LRG) sample from the DR9 DESI Legacy Survey and the *Planck* PR4 CMB lensing maps to constrain the local primordial non-Gaussianity parameter $f_{\rm NL}$ using the scale-dependent galaxy bias effect. The galaxy sample covers $\sim 40\%$ of the sky and contains galaxies up to $z \sim 1.4$, and is calibrated with the LRG spectra that have been observed for the DESI Survey Validation.

Methods. We apply a nonlinear imaging systematics treatment based on neural networks to remove observational effects that could potentially bias the $f_{\rm NL}$ measurement. Our measurement is performed without blinding, but the full analysis pipeline is tested with simulations including systematics.

Results. Using the two-point angular cross-correlation between LRG and CMB lensing only ($C_\ell^{\kappa G}$) we find $f_{\rm NL} = 39^{+40}_{-38}$ at 68% confidence level, and our result is robust in terms of systematics and cosmology assumptions. If we combine this information with the autocorrelation of LRG (C_ℓ^{GG}) applying a $\ell_{\rm min}$ scale cut to limit the impact of systematics, we find $f_{\rm NL} = 24^{+20}_{-21}$ at 68% confidence level. Our results motivate the use of CMB lensing cross-correlations for measuring $f_{\rm NL}$ with future datasets given its stability in terms of observational systematics compared to the angular auto-correlation.

Key words. Cosmology: large-scale structure of Universe – CMB cross-correlations – primordial non-Gaussianity

1. Introduction

Cosmic inflation was proposed as a theory in the early 1980s (Guth 1981; Starobinsky 1980). The inflation framework was initially formulated to solve Big Bang problems such as the horizon, flatness and magnetic monopole problems; however, inflation is also able to explain the formation of primordial density perturbations (Starobinsky 1982; Guth & Pi 1985; Bardeen et al. 1983). Inflation is defined as a phase in which the Universe is expanding exponentially, driven by a scalar field ϕ. Several models of inflation have been proposed in the literature (see e.g. Langlois 2010; Vazquez Gonzalez et al. 2020 for a review). The model of inflation and its predictions is defined by choosing the form of the potential $V(\phi)$. The simplest inflationary models predict Gaussian initial conditions; however, alternative inflationary models predict different levels of non-Gaussianity in the primordial density perturbations (Chen 2010; Takahashi 2014). The level of non-Gaussianity has been usually characterized in the literature with the $f_{\rm NL}$ non-Gaussianity parameter, such that detecting $f_{\rm NL} \neq 0$ is a signature of having non-Gaussian initial conditions.

The tightest constraint on $f_{\rm NL}$ is currently provided by the measurements from the CMB bispectrum. Using *Planck* 2018 data, a value $f_{\rm NL} = -0.9 \pm 5.1$ at 68% confidence level was found (Planck Collaboration et al. 2019). However, Dalal et al. (2008) first noticed that local non-Gaussian initial conditions lead to a characteristic scale-dependent signature in the galaxy bias, following a $1/k^2$ scale-dependence in the ratio between the total matter to observed density of galaxies. During the last decade, many works have performed measurements from the large scale structure using the scale-dependent bias effect (Ross et al. 2012; Castorina et al. 2019; Mueller et al. 2021; Cabass et al. 2022; D'Amico et al. 2023, among others). In the last years, some measurements from LSS using the scale-dependent galaxy bias have been achieved using the eBOSS DR16 quasars: Mueller et al. (2021) measured $f_{\rm NL} = -12 \pm 21$ and Cagliari et al. (2023) obtained $-4 < f_{\rm NL} < 27$ using different methodologies. More recently, Chaussidon et al. (2024) improved this constraint to $f_{\rm NL} = -3.6^{+9.1}_{-9.0}$ using the 3D power spectrum of DESI DR1 galaxies and quasars. This is a challenging measurement because it requires very accurate control of the largest scales where the scale-dependent bias effect due to $f_{\rm NL}$ arises. Further, it is also important to mention than when performing $f_{\rm NL}$ measurements

⋆ e-mail: jrbermejo@iac.es

from LSS, unless doing certain assumptions we actually measure the product of $f_{\rm NL}$ times an unknown bias (see Sec. 2.1 for more details).

The Dark Energy Spectroscopic Instrument (DESI, Levi et al. 2013) is a spectroscopic survey that is being carried out currently from the 4m Mayall telescope at Kitt Peak National Observatory (AZ, USA). Its unique design with 5000 fibers with robotic positioners allows to take thousands of spectra in a single exposure (DESI Collaboration et al. 2016a, 2022; Silber et al. 2023; Miller et al. 2024; Guy et al. 2023; Schlafly et al. 2023). Theoretical forecasts (DESI Collaboration et al. 2016b) expect the full 5-year survey will have the capability to achieve a sensitivity $\sigma(f_{\rm NL}) \sim 5$, similar to the best current CMB bispectrum constraint, if there is a good control of systematic effects. Before the first spectroscopic data releases (DESI Collaboration et al. 2023, 2024a) and science results (DESI Collaboration et al. 2024d,c,b,e,f) came out, a full imaging survey was performed in order to select the spectroscopic targets. This targeting survey is called the DESI Legacy Survey (Dey et al. 2019) and covers a broad area ($\gtrsim$20000 deg^2), making it useful for measuring $f_{\rm NL}$ using the scale-dependent galaxy bias. Two previous works have already used the DESI Legacy Survey information to put a constraint on $f_{\rm NL}$: Rezaie et al. (2023) used the angular power spectra of the LRG targets, and Krolewski et al. (2024) used the cross-correlation between quasar targets and the *Planck* CMB lensing.

CMB lensing describes the remapping of the CMB anisotropies due to gravitational lensing by structures along the line of slight. The CMB lensing potential can be easily measured from the observations of the lensed sky (Hu & Okamoto 2002) and was first detected by Smith et al. (2007). Since it contains information about the large scale structure geometry, its cross-correlation with galaxy tracers can be useful to constrain cosmology. Although CMB lensing and galaxy tracers probe the same structures, they are affected by different systematics, making the cross-correlation between the two a powerful additional tool for measurements into the systematics-dominated regime. Several authors have stressed using theoretical forecasts the capabilities of the cross-correlation between CMB lensing and galaxy matter tracers to better constrain $f_{\rm NL}$ (e.g. Schmittfull & Seljak 2018; Giusarma et al. 2018; Ballardini et al. 2019; Bermejo-Climent et al. 2021). More recently, Krolewski et al. (2024) found $f_{\rm NL} = -26^{+45}_{-40}$ using the cross-correlation between *Planck* lensing and DESI quasar targets. Additionally, recent data analysis works have been performed to constrain other cosmological parameters such as the amplitude of matter density fluctuations, commonly parametrized in terms of σ_8 (the RMS density contrast smoothed on a scale of 8 h/Mpc), and matter density $\Omega_{\rm m}$ using CMB cross-correlations with the DESI Legacy Survey (e.g. White et al. 2022a, Sailer et al. 2024; Kim et al. 2024).

In this paper, we intend to extend the analysis done in Rezaie et al. (2023) with the DESI LRG sample to the inclusion of the CMB lensing cross-correlation as additional information and technique to limit the impact of observational systematics. In Rezaie et al. (2023) an extensive and detailed effort was performed in order to remove observational systematics which could bias the PNG measurement. Nonetheless, they concluded their results motivate further studies of PNG with samples less sensitive to systematics like LRG spectroscopic data. Here, our aim is to explore the capability of CMB lensing - LRG cross-correlation to constrain $f_{\rm NL}$ and its stability in terms of systematics, alone and in combination with the LRG auto-correlation.

This paper is organized as follows: In Sec. 2 we review the theoretical framework for the imprints of $f_{\rm NL}$ in a scale-dependent galaxy bias and for the cosmological observables we study in the angular domain. In Sec. 3 we present the DESI LRG and *Planck* lensing datasets used for our analysis. In Sec. 4 we describe the pipeline followed for treating our datasets including a systematics mitigation, computation of observables and parameter inference. In Sec. 5 we discuss a validation of our analysis pipeline with mock LRG and CMB lensing fields. In Sec. 6 we present our results for the measurement of PNG and some robustness tests, and in Sec. 7 we summarize our conclusions.

2. Theory

In this section we first provide a description of the physical model that originates a scale-dependent galaxy bias due to a local PNG and then describe the cosmological observables in the 2D harmonic space involved in our analysis.

2.1. Primordial non-Gaussianity and scale dependent bias

If we assume a type of non-Gaussianity that depends only on the local value of the potential, the parametrization of the primordial potential can be written as follows (Komatsu & Spergel 2001)

$$\Phi = \phi + f_{\rm NL}(\phi^2 - \langle\phi\rangle^2)\,, \tag{1}$$

where $f_{\rm NL}$ is the parameter that describes the amplitude of the quadratic non-Gaussian term, and ϕ is a random Gaussian field.

We study $f_{\rm NL}$ through its impact on the scale-dependent galaxy bias as introduced in Dalal et al. (2008). If we assume the so-called universality relation (Slosar et al. 2008) the contribution to the galaxy bias is expressed as

$$\Delta b(k,z) = 2(b_g - p) f_{\rm NL} \frac{\delta_{\rm crit}}{\alpha(k)}\,, \tag{2}$$

where $\delta_{\rm crit} = 1.686$ is the threshold overdensity for spherical collapse, b_g is the z-dependent galaxy bias, $p \simeq 1$ for the case of LRG and $\alpha(k)$ is the relation between potential and density field, such that $\delta(k) = \alpha(k)\Phi(k)$. The value of $\alpha(k)$ is given by

$$\alpha(k) = \frac{2k^2 T(k) D(z)}{3\Omega_{\rm m}} \frac{c^2}{H_0^2} \frac{g(0)}{g(\infty)}\,, \tag{3}$$

where $T(k)$ is the transfer function, $D(z)$ is the growth factor (normalized to be 1 at $z = 0$), $\Omega_{\rm m}$ the matter density, and the factor $g(\infty)/g(0) \simeq 1.3$ accounts for the different normalizations of $D(z)$ in the CMB and LSS literature. This definition of $f_{\rm NL}$ is therefore the so-called 'CMB convention'. Other authors (e.g. Carbone et al. 2008; Afshordi & Tolley 2008; Grossi et al. 2009) refer to the use of the 'LSS convention', where the $g(\infty)/g(0)$ factor is absorbed into the definition of $f_{\rm NL}$, such that $f_{\rm NL}^{\rm LSS} \simeq 1.3 f_{\rm NL}^{\rm CMB}$. Note that even if we assume $p = 1$, many works based on dark-matter-only simulations (e.g. Adame et al. 2024) have found significant deviations from $p = 1$. In this direction, other authors (e.g. Barreira 2020, 2022) have stressed that we can only constrain the product $b_\phi f_{\rm NL}$ through the scale-dependent bias effect, where b_ϕ is a parameter usually defined as $b_\phi = 2\delta_{\rm crit}(b_g - p)$, in order to account for the uncertainties on p.

2.2. Cosmological observables

In this work we focus on the angular power spectrum of the galaxy - CMB lensing cross-correlation, $C_\ell^{\kappa G}$ as well as the galaxy autocorrelation C_ℓ^{GG}.

The angular power spectrum can be calculated as

$$C_\ell^{XY} = 4\pi \int \frac{\mathrm{d}k}{k} \mathcal{P}(k) I_\ell^X(k) I_\ell^Y(k) \tag{4}$$

where $\mathcal{P}(k) \equiv k^3 P(k)/(2\pi^2)$ is the dimensionless primordial power spectrum and $I_\ell^X(k)$ is the kernel for the X field for unit primordial power spectrum.

All the weak lensing quantities can be defined from the lensing potential

$$\phi(\hat{\mathbf{n}}, \chi) = \frac{2}{c^2} \int_0^\chi \mathrm{d}\chi' \frac{\chi - \chi'}{\chi\chi'} \Phi(\chi'\hat{\mathbf{n}}, \chi') \tag{5}$$

where $\Phi(\hat{\mathbf{n}}, \chi)$ is the gravitational potential. The comoving distance is

$$\chi(z) = \int_0^z \frac{c\,\mathrm{d}z'}{H(z')} . \tag{6}$$

The observable 2-dimensional lensing potential, averaged over background sources with a redshift distribution $W_b(\chi)$, is given by

$$\phi(\hat{\mathbf{n}}) = \frac{2}{c^2} \int_0^\chi \frac{\mathrm{d}\chi'}{\chi'} q_b(\chi') \Phi(\chi'\hat{\mathbf{n}}, \chi') \tag{7}$$

where $q_b(\chi)$ is the lensing efficiency (for a given background distribution W_b) defined as

$$q_b(\chi) = \int_0^\chi \mathrm{d}\chi' \frac{\chi' - \chi}{\chi'} W_b(\chi') . \tag{8}$$

By expanding the gravitational potential in Fourier space and using the plane-wave expansion, we can define the lensing potential kernel as

$$I_\ell^\phi(k) = 2\left(\frac{3\Omega_m H_0^2}{2k^2c^2}\right) \int \frac{\mathrm{d}\chi}{(2\pi)^{3/2}} \frac{q_b(\chi)}{\chi a(\chi)} j_\ell(k\chi)\, \delta(k, \chi) , \tag{9}$$

where Ω_m is the present-day matter density, H_0 is the Hubble constant, $\delta(k, \chi)$ is the comoving-gauge linear matter density perturbation, and j_ℓ the spherical Bessel functions. In case of CMB lensing, the source distribution can be approximated by $W_{\rm CMB}(\chi) \simeq \delta_{\rm D}(\chi - \chi_*)$ and the lensing efficiency by

$$q_{\rm CMB}(\chi) \simeq \frac{\chi_* - \chi}{\chi_*} \tag{10}$$

where χ_* is the comoving distance at the surface of last scattering, and Eq. (9) reduces to

$$I_\ell^{\phi_{\rm CMB}}(k) = 2\left(\frac{3\Omega_m H_0^2}{2k^2c^2}\right) \int \frac{\mathrm{d}\chi}{(2\pi)^{3/2}} \frac{\chi_* - \chi}{\chi_*\chi} \frac{1}{a(\chi)} j_\ell(k\chi)\, \delta(k, \chi) . \tag{11}$$

Finally the convergence $\kappa = \nabla^2\phi/2$ can be expanded in spherical-harmonics as

$$\kappa(\hat{\mathbf{n}}) = -\frac{1}{2} \sum_{\ell,m} \ell(\ell+1) \phi_{\ell m} Y_\ell^m(\hat{\mathbf{n}}) \tag{12}$$

and we can relate the two kernel by

$$I_\ell^\kappa(k) = \frac{\ell(\ell+1)}{2} I_\ell^\phi(k) . \tag{13}$$

The 2-dimensional integrate window function for the galaxy number counts is

$$I_\ell^G(k) = \int \frac{\mathrm{d}\chi}{(2\pi)^{3/2}} W(\chi) \Delta_\ell(k, \chi) \tag{14}$$

where $\Delta_\ell(k, \chi)$ is the observed number counts and $W(\chi)$ is a window function given by the redshift distribution of galaxies. At first order, the most important contribution to $\Delta_\ell(k, \chi)$ is given by the synchronous gauge source counts Fourier transformed and expanded into multipoles, $\Delta_\ell^s(k, \chi)$. We assume that $\Delta_\ell^s(k, \chi)$ is related to the underlying matter density field through a scale and redshift dependent galaxy bias b_g as

$$\Delta_\ell^s(k, \chi) = b_g(k, \chi) \delta(k, \chi) j_\ell(k\chi) . \tag{15}$$

where $b_g(k, \chi)$ is given by the sum of a linear bias, which is not scale dependent, plus the scale dependent contribution given by Eq. 2. We also consider nonlinear contributions to the power spectrum using `halofit` (Takahashi et al. 2012). In this paper, we will also consider two important contributions to the total observed number counts: the effects of redshift space dirtortions (RSD) and lensing magnification (see Fig. 4 for more details). The RSD term is given by

$$\Delta_\ell^{\rm RSD}(k, \chi) = \frac{k v_k}{\mathcal{H}} j_\ell''(k\chi) \tag{16}$$

where v_k is the velocity of the sources and $\mathcal{H}$ is the Hubble parameter. The lensing convergence contribution is given by

$$\Delta_\ell^{\rm lensing}(k, \chi) = \ell(\ell+1)(2 - 5s) \int_0^\chi \mathrm{d}\chi' \frac{\chi - \chi'}{\chi\chi'} \Phi(\chi'\hat{\mathbf{n}}, \chi') \tag{17}$$

where s is the magnification bias, which accounts for the fact that observed galaxies are magnified by gravitational lensing. Note that there are other contributions from General Relativity to the number counts, but we consider them of second order since the most important contribution to $C_\ell^{\kappa G}$ is the lensing magnification (see e.g. Appendix A of Bermejo-Climent et al. 2021)

3. Datasets

We describe in this section the datasets involved in our analysis. The two main ingredients are a Luminous Red Galaxies (LRG) photometric catalog from the DR9 Legacy Survey (Zhou et al. 2023b) and the *Planck* PR4 public CMB lensing maps (Carron et al. 2022). We also use a LRG spectroscopic sample from the DESI Survey Validation data to calibrate the redshift distribution of the photometric DESI LRG.

3.1. Luminous Red Galaxies

Our galaxy sample consists of a Luminous Red Galaxies (LRG) catalog obtained from the DESI Imaging Legacy Surveys[1] Data Release 9 (DR9, Dey et al. 2019). These surveys were a combination of three projects: the Dark Energy Camera Legacy Survey using the Blanco 4m telescope in Chile (DECaLS, Flaugher et al. 2015), the Beijing-Arizona Sky Survey using the Bok telescope at Kitt Peak (BASS, Zou et al. 2017) and the Mayall z-band Legacy Survey (MzLS, Dey et al. 2019) using the Mayall telescope at Kitt Peak. BASS and MzLS observed the same region in the North galactic cap, while DECaLS observed in both the North and South galactic caps. The combination of the three

[1] https://www.legacysurvey.org/

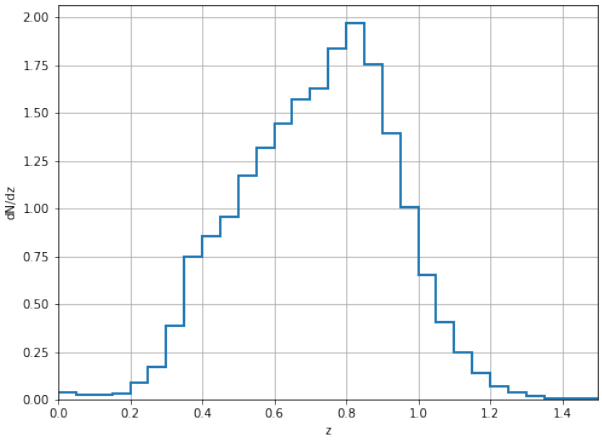

Fig. 1. Normalized redshift distribution of the LRG sample, directly measured using the spectroscopic redshifts from DESI Y1 data.

projects covered ∼19000 deg^2 in the sky to select the spectroscopic targets that are being currently observed with DESI.

We calibrate the redshift distribution, dN/dz, of the sample using the actual LRG spectra measured with DESI Survey Validation (DESI Collaboration et al. 2023, 2024a). In Fig. 1 we show the redshift distribution of the sample as obtained from the LRG spectra. These spectra are not available for declinations lower than $-30°$, hence, we remove the DEC $< -30°$ region from the photometric LRG footprint. In Zhou et al. (2023b) they also described the presence of a photometric zero-point systematic effect at low declinations. The resulting final sample contains around ∼ 9 million galaxies covering a ∼16000 deg^2 area. Then, we apply to the LRG catalog the mask designed in Zhou et al. (2023a) to reduce contamination from effects such as stars and foregrounds. We pixelize the LRG catalog converting it into a HEALPix (Gorski et al. 2005) galaxy counts map at $N_{\rm side} = 256$. This map is corrected for the pixel incompleteness effect, which accounts for area losses on scales smaller than a $N_{\rm side} = 256$ healpix pixel, such as cutouts around bright stars. Finally, the galaxy counts map can be easily converted into an overdensity field by normalizing and substracting the mean density. We show the LRG overdensity field in Fig. 2.

We note that since this sample contains photometric redshifts, one could design optimal weights in order to enhance the $f_{\rm NL}$ signal by emphasizing the higher redshift part of the LRG sample. We do not perform this kind of analysis here since we consider it is beyond the scope of this paper.

3.2. CMB lensing

The other ingredient in our analysis is the *Planck* CMB lensing potential map. We use the *Planck* PR4 reconstruction of the CMB lensing potential (Carron et al. 2022), which was obtained from the *Planck* NPIPE temperature and polarization maps (Akrami et al. 2020). In particular, we use the minimum-variance estimate from temperature and polarization, after mean-field subtraction of the lensing convergence. This latest release of CMB lensing maps improves the noise with respect to the previous *Planck* PR3 maps (Planck Collaboration et al. 2020); in particular, the large scale noise is lower and the mean-field is better understood thanks to the larger number of simulations. The maps and the mask are publicly available[2]. We show the CMB lensing field in Fig 2.

Note that the CMB lensing map does not have the Monte Carlo multiplicative correction applied in (Carron et al. 2022). We compute this correction based on simulations as in Krolewski et al. (2024) using mode decoupled pseudo-C_ℓ, and apply the result as a multiplicative factor to the measured cross-correlation angular power spectra $C_\ell^{\kappa G}$. This correction can not applied in a general way, since it depends on the footprint mask for each tracer involved in the analysis due to local variations of the normalization. The order of this correction is generally $\lesssim 5\%$, but it becames larger (∼10-12%) for the largest scales, having thus a non negligible impact on the $f_{\rm NL}$ measurements.

4. Analysis pipeline

We describe in this section the pipeline implemented to analyze the LRG and CMB lensing HEALPix maps. The first step is to apply an imaging systematics mitigation code to the LRG maps. This mitigation treatment operates at the map level and returns a series of systematic weights for each pixel that are applied to the raw LRG maps. Then, we compute the angular power spectrum C_ℓ of the LRG their cross-correlation with the *Planck* lensing, as well as the covariance matrices. The final step is to perform a Monte-Carlo Markov Chain based parameter inference to constrain $f_{\rm NL}$.

4.1. Imaging systematics mitigation

Imaging systematics due to effects such as extinction, stellar contamination or changes in the observational conditions usually generate an excess of power at large scales (low multipoles), where the $f_{\rm NL}$ signal arises. Thus, an efficient imaging systematics treatment is key for measuring an unbiased $f_{\rm NL}$. Rezaie et al. (2020) presented a neural network approach for systematics mitigation as a way to model the relation between the observed galaxy density fields and the imaging systematics templates. This pipeline is implemented in the `SYSnet` code, which is publicly available[3]. In Rezaie et al. (2023), a detailed study of the performance of `SYSnet` was done using this LRG sample, with the aim of measuring $f_{\rm NL}$ from the C_ℓ^{GG} autospectra. A different number of approaches were explored, given that `SYSnet` can return different results depending on the selection of features (imaging systematics templates maps) used to perform the regression.

In this paper, we intend to use a mitigation recipe optimized for measurements from the cross-correlation between the DESI LRG and *Planck* lensing, $C_\ell^{\kappa G}$. At first order, the cross-correlation itself as a technique would be enough to remove the effects of the systematics if we assume there are not any correlated systematics between the CMB lensing and LRG maps. However, there could still be potential correlated systematics due to galatic foregrounds that affect both probes. Furthermore, the noise in C_ℓ^{GG} contributes to the $C_\ell^{\kappa G}$ covariance matrix: systematics affecting the C_ℓ^{GG} power spectrum would also lead to an increase of the $C_\ell^{\kappa G}$ covariance, and as a result larger uncertainties on $f_{\rm NL}$. At the same time, a very aggressive mitigation recipe could remove real clustering signal and overfit the $C_\ell^{\kappa G}$ power spectrum, biasing the $f_{\rm NL}$ measurements towards lower values. For this reason, in order to find a compromise between removing the excess of power spectrum due to systematics for

[2] https://github.com/carronj/planck_PR4_lensing/releases/tag/Data
[3] https://github.com/mehdirezaie/SYSNet

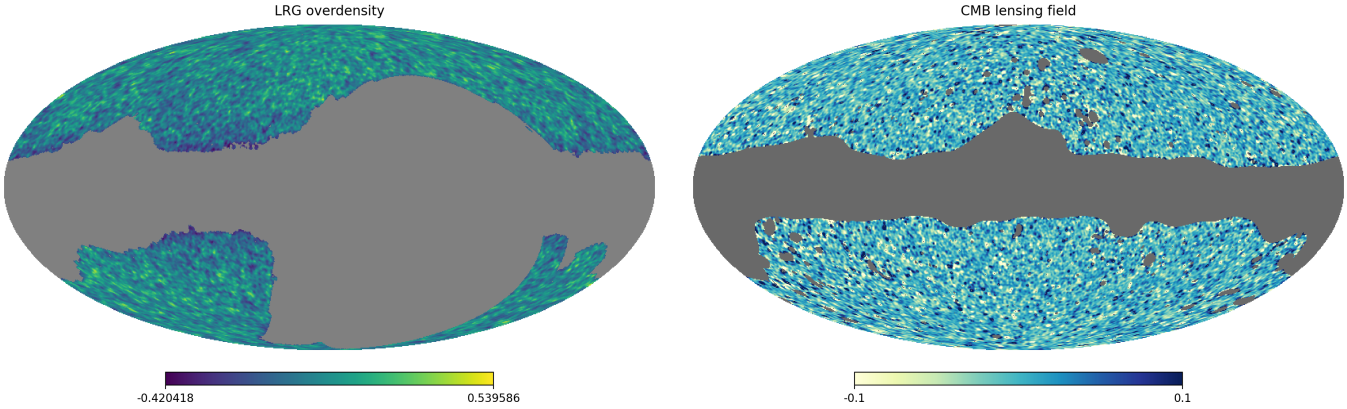

Fig. 2. Left panel: LRG overdensity field in galactic coordinates, after applying the δ < -30º cut. Right panel: CMB lensing field in galactic coordinates obtained from the *Planck* PR4 maps.

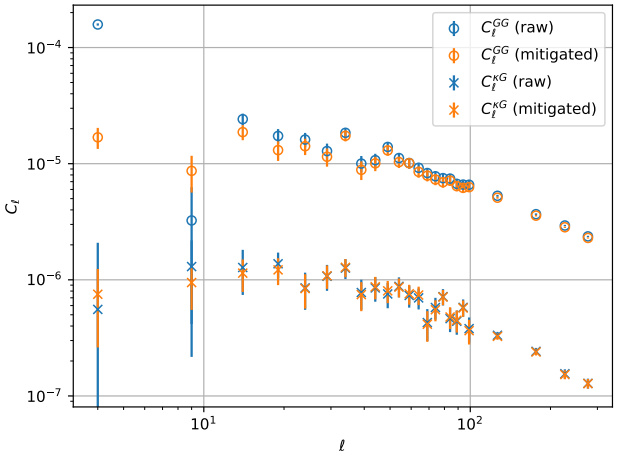

Fig. 3. Angular power spectra of the LRG autocorrelation, C_ℓ^{GG}, and CMB lensing - LRG cross-correlation, $C_\ell^{\kappa G}$, obtained from the raw (uncorrected) data and after applying the systematics mitigation pipeline to the LRG maps.

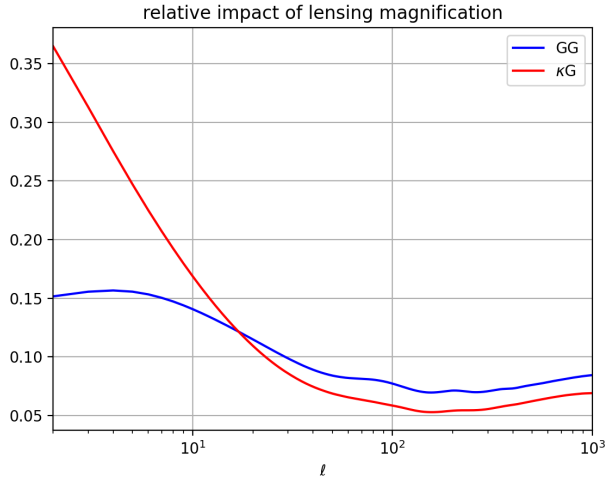

Fig. 4. Relative impact of the lensing magnification contribution for the C_ℓ^{GG} (blue line) and $C_\ell^{\kappa G}$ (red line) theoretical angular power spectra obtained with `CAMB`.

C_ℓ^{GG} and avoiding a strong overfit of $C_\ell^{\kappa G}$, we select the *Nonlinear Three Maps* recipe from Rezaie et al. (2023). This choice is the most conservative one among the recipes applied in Rezaie et al. (2023) with the `SYSnet` code, and relies of selecting three features or systematics templates for the regression: extinction, galactic depth in z-band and PSF size in r-band. We refer the reader to Rezaie et al. (2023) for more details about the different possibilities of feature selections. In Sec. 5 we also show this prescription provides unbiased measurements of the angular power spectrum on contaminated mocks.

4.2. Angular power spectra and covariance matrix

In order to estimate the angular power spectra of the LRG autocorrelation and their cross-correlation with the *Planck* lensing, we use the pseudo-C_ℓ approach implemented in the publicly available `NaMaster` code by Alonso et al. (2019). The pseudo-C_ℓ of a pair of fields can be defined as

$$\tilde{C}_\ell^{XY} = \frac{1}{2\ell+1}\sum_m X_{\ell m} Y_{\ell m}^* \tag{18}$$

where X, Y are the observed fields. Then, the difference between the true and measured C_ℓ due to the effects of the mask is accounted through the mode-coupling matrix $M_{\ell\ell'}$ as

$$\langle \tilde{C}_\ell \rangle = \sum_{\ell'} M_{\ell\ell'} C_{\ell'} \,. \tag{19}$$

In our case, we directly apply to the observed LRG density a completeness mask, so we just deconvolve the binary footprint mask. In practice, the inversion of the $M_{\ell\ell'}$ matrix is done using the MASTER algorithm (Hivon et al. 2002), which requires a discrete binning of the angular power spectrum. We use the implementation in the `compute_full_master` function from the `NaMaster` code to calculate $C_\ell^{\kappa G}$ and C_ℓ^{GG}. We bin the theory curves using the same bandpower window functions.

As scale cuts, for $C_\ell^{\kappa G}$we adopt $\ell_{\rm min} = 2$ and $\ell_{\rm max} = 300$, and we bin the power spectra using $\Delta\ell = 5$ for $\ell < 100$ and $\Delta\ell = 50$ for $\ell > 100$. The reason to use this scheme is to set a good sampling of the angular power spectra at large scales where the $f_{\rm NL}$ signal arises, and the $\ell_{\rm max} = 300$ is safe enough to minimize the limitations of modeling the nonlinear scales, which could potentially affect the measurement of the linear bias. We checked with mock fields that the results are stable with both $N_{\rm side}$ and

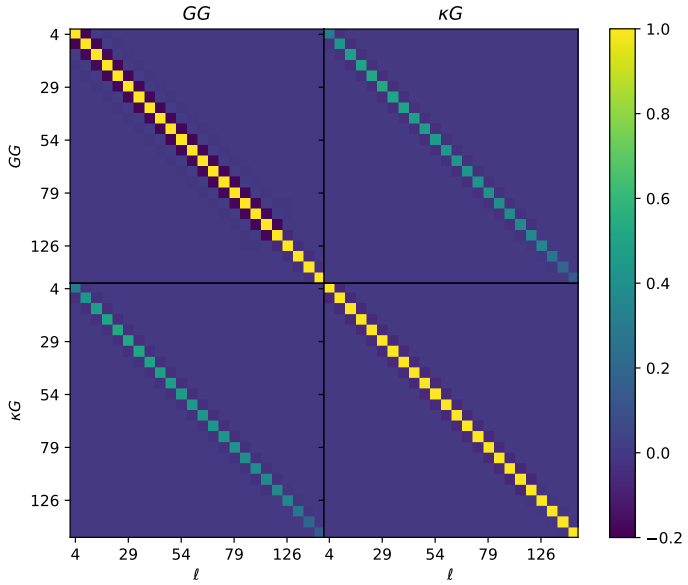

Fig. 5. Correlation matrix as obtained from the joint covariance matrix for C_ℓ^{GG} and $C_\ell^{\kappa G}$ computed with the `NaMaster` code.

$\ell_{\rm max}$ (see Sec. 5 for more details about the mocks). For C_ℓ^{GG}, we implement the same multipole binning scheme, but we drop out the first multipole bin of the analysis and set $\ell_{\rm min} = 7$. The motivation for this choice is to use a scale cut for C_ℓ^{GG} that limits the impact of remaining systematics according to the mitigation pipeline tests on mocks (see Sec. 5 for more details).

We show in Fig. 3 the measured power spectra of the LRG autocorrelation C_ℓ^{GG} and its cross-correlation with the *Planck* lensing $C_\ell^{\kappa G}$, obtained using uncorrected (raw) LRG maps and mitigated LRG maps with the neural network pipeline.

For the covariance matrices, we use the analytic `gaussian_covariance` function in `NaMaster` (García-García et al. 2019) to compute the full Gaussian covariance for a masked field. We account for the potential extra power in C_ℓ^{GG} due to systematics by smoothing the measured angular power spectra from the data and using it as input for the covariance matrix computation. As a test, we also compute the covariance using mock fields obtaining compatible results. More details of the mock fields used can be found in Sec. 5. We show in Fig. 5 the computed joint correlation matrix for C_ℓ^{GG} and $C_\ell^{\kappa G}$.

4.3. Likelihood and parameter inference

We define the likelihood $\mathcal{L}$ as

$$-2\log\mathcal{L} \equiv \chi^2 = \sum_{\ell,\ell'} \left(C_\ell^{\rm obs} - \tilde{C}_\ell(\theta)\right) {\rm Cov}^{-1}_{\ell\ell'} \left(C_{\ell'}^{\rm obs} - \tilde{C}_{\ell'}(\theta)\right) \quad (20)$$

where $C_\ell^{\rm obs}$ are the elements the data vector, $\tilde{C}_\ell(\theta)$ is the theoretical model of the angular power spectrum for a given set of parameters θ and ${\rm Cov}^{-1}$ is the inverse of the covariance matrix.

Our theoretical model is based in the Code for Anisotropies in the Microwave Background, `CAMB` (Lewis & Challinor 2011). This code is publicly available[4] and allows the computation of the angular power spectra of the CMB fields and also galaxy fields, given a window function determined by the galaxy bias b_g and the redshift distribution ${\rm d}N/{\rm d}z$. We slightly modify the code to include the scale dependence of the galaxy bias induced by $f_{\rm NL}$. The ${\rm d}N/{\rm d}z$ is directly measured using the DESI LRG spectra from Survey Validation (DESI Collaboration et al. 2023, 2024a). The rest of the fiducial cosmological parameters in `CAMB` are fixed to the *Planck* 2018 bestfit estimations (Planck Collaboration et al. 2020), except for σ_8, which we set to a fiducial value $\sigma_8 = 0.77$ to be in agreement with the measurements from the cross-correlation between ACT lensing and this LRG sample (Sailer et al. 2024; Kim et al. 2024).

In the computation of the theoretical angular power spectra with the `CAMB` code, we include the lensing magnification contribution to the galaxy number counts. This effect accounts for the fact that the light from distant galaxies is affected by the structures along the line of sight, resulting in an increased flux. The lensing magnification contribution to the angular power spectra can be included in `CAMB` once we specify the magnification bias s as an input parameter. This parameter depends on the galaxy tracer, and for this LRG sample, we fix the magnification bias value to $s = 0.999$ as determined in Kitanidis & White (2021). More recent measurements using this sample split in four redshift bins (White et al. 2022b; Zhou et al. 2023b) have found compatible results within the uncertainty for the various redshift bins, hence, we consider safe enough the assumption of a z-independent value for s. In Fig. 4 we show the relative importance of the lensing magnification contribution to the C_ℓ^{GG} and $C_\ell^{\kappa G}$ theoretical angular power spectra obtained with `CAMB`. The impact at the lowest multipoles can reach up to $\sim 15\%$ for the LRG autocorrelation and $\sim 35\%$ for the LRG - CMB lensing cross-correlation, hence, this effect is not negligible in our theoretical model for this tracer.

To compute the constraints on the cosmological parameters, we implement our likelihood using the Monte Carlo Markov Chain (MCMC) sampler `emcee`[5] (Foreman-Mackey et al. 2013). Our analysis includes $f_{\rm NL}$ and the galaxy bias at $z = 0$, b_0, as the two main cosmological parameters of interest to constrain. We assume a fiducial redshift evolution of the galaxy bias following

$$b_g = b_0 \times D(z)^{-1} \quad (21)$$

where $D(z)$ is the growth factor normalized to be 1 at $z = 0$. This choice is motivated by the analysis in Zhou et al. (2021), where a bias evolution compatible with $b(z) \simeq 1.5/D(z)$ was found for the DESI LRG targets. For C_ℓ^{GG}, we also consider the shot noise $N_{\rm shot}$ as a nuisance parameter. We do not impose any prior knowledge on the b_0 and $N_{\rm shot}$ parameters, but restrict their sampling to positive values to avoid nonphysical results.

5. Validation with mocks

Before applying the analysis pipeline described in the previous section to the real LRG and CMB lensing data, we test it with mock Gaussian fields that simulate the DESI Legacy Survey LRG sample and the *Planck* lensing observations. For the LRG, we use a sample of 100 Gaussian fields for $f_{\rm NL} = 0$, 50 and -50. For the CMB lensing, we use a set of 100 correlated maps. These correlated fields are generated using the `healpy`[6] Python package in the following way:

– We first use `CAMB` to compute the theoretical angular power spectra C_ℓ^{GG}, $C_\ell^{\kappa G}$ and $C_\ell^{\kappa\kappa}$, given the redshift window function ${\rm d}N/{\rm d}z$ obtained from the spectroscopic LRG redshift distrubution and the different values of $f_{\rm NL}$. The galaxy bias parameter at $z = 0$ is set to a fiducial value of $b_0 = 1.5$ based

[4] https://camb.info/

[5] https://emcee.readthedocs.io/

[6] https://github.com/healpy

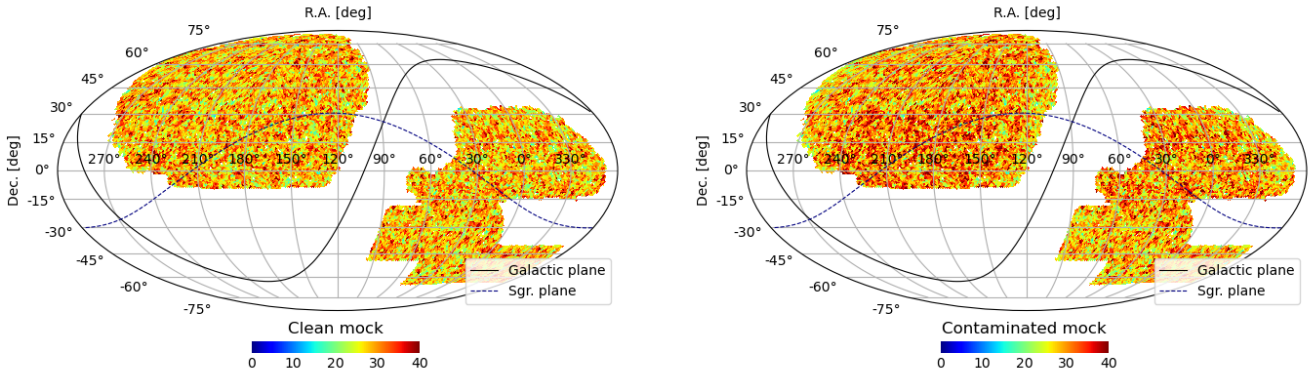

Fig. 6. A single gaussian realization of a LRG map before adding contamination (left panel) and after applying `regressis` to contaminate the mock (right panel).

on Zhou et al. (2021). The fiducial cosmological parameters are set according to the *Planck* 2018 measurements (Planck Collaboration et al. 2020).

– The theoretical angular power spectra are used as input for the `healpy.synfast` function. Following the recipe in Giannantonio et al. (2008); Serra et al. (2014) for simulating correlated fields, we first build a CMB lensing map with a given seed and power spectrum $C_\ell^{\kappa\kappa}$. Then, we generate another map with the same seed and power spectrum $(C_\ell^{\kappa G})^2/C_\ell^{\kappa\kappa}$, and we add to this last map another component with a different seed and power spectrum $C_\ell^{GG} - (C_\ell^{\kappa G})^2/C_\ell^{\kappa\kappa}$. These maps will have amplitudes given by

$$\begin{aligned} a_{\ell m}^{\kappa\kappa} &= \xi_1 (C_\ell^{\kappa\kappa})^{1/2} \\ a_{\ell m}^{GG} &= \xi_1 C_\ell^{\kappa G}/(C_\ell^{\kappa\kappa})^{1/2} + \xi_2 \left(C_\ell^{GG} - (C_\ell^{\kappa G})^2/C_\ell^{\kappa\kappa}\right)^{1/2} \end{aligned} \tag{22}$$

where ξ_1, ξ_2 are random amplitudes, i. e. complex numbers with zero mean and unity variance. It is easy to show that:

$$\begin{aligned} \langle a_{\ell m}^{\kappa\kappa} a_{\ell m}^{\kappa\kappa *}\rangle &= C_\ell^{\kappa\kappa}, \\ \langle a_{\ell m}^{\kappa\kappa} a_{\ell m}^{GG *}\rangle &= C_\ell^{\kappa G}, \\ \langle a_{\ell m}^{GG} a_{\ell m}^{GG *}\rangle &= C_\ell^{GG}. \end{aligned} \tag{23}$$

The output products are a subsample of 100 mock CMB lensing fields and 100 correlated LRG overdensity fields with $N_{\rm side} = 256$ for each value of $f_{\rm NL}$. We finally apply to the mocks the same masks we use for the LRG and CMB lensing data.

In order to test the performance of the systematics mitigation pipeline, we contaminate the LRG maps. For this purpose, after generating the mock LRG and CMB lensing fields, we use the `regressis`[7] code (Chaussidon et al. 2021) and the following procedure:

– From the LRG density fields, we simulate LRG discrete number counts maps using Poisson sampling based on the expected LRG density for each pixel. This procedure is safe enough due to the low map resolution, which makes unlikely to get pixels with predicted density lower than 0 for the Gaussian fields. We also checked the angular power spectra are in agreement with the input after Poisson sampling.

[7] https://github.com/echaussidon/regressis

– We generate "high density" simulated LRG maps by duplicating the number of objects per pixel. Then, we create a mock LRG catalog by assigning random coordinates within a given pixel to each galaxy.

– The "high density" catalog is used as input for `regressis`. Basing on the systematics weights, which are estimated from running SYSnet on the real data, the code creates a contaminated mock catalog by removing galaxies and matching the final catalog to the expected LRG density. The result is converted back into a contaminated map.

Note that we do not add any contamination to the CMB lensing mock fields: this is equivalent to assuming there is no correlation in systematics between the two probes, and the main purpose of this test is to check whether the systematics mitigation removes real cross-correlation signal in the $C_\ell^{\kappa G}$ power spectra.

We show in Fig. 6 an example of a clean mock map and the same contaminated mock map after applying `regressis`. These contaminated maps are used as input for `SYSNet`, the neural network code for systematics mitigation described in Sect. 4.1. For each realization, we apply `SYSNet` separately in three different regions of the sky: one corresponding to the BASS and MzLS footprints, and two corresponding to DECaLS in the North and South galactic caps (see Fig. 2 of Rezaie et al. 2023). After recombining the output in a single map, we compute the angular power spectra of the lensing - LRG cross-correlation $C_\ell^{\kappa G}$ and the LRG autocorrelation C_ℓ^{GG} for the mocks without the contamination (clean power spectrum), then we add the contamination and finally apply the systematics weights obtained with `SYSNet`.

The comparison of angular power spectra is shown in Fig. 7. For $C_\ell^{\kappa G}$, we find no significant differences between the contaminated and true power spectra. While the mitigated spectra is systematically lower than the truth, this difference is smaller than the dispersion of the clean mocks power spectra (i.e. the $C_\ell^{\kappa g}$ uncertainty). In relative terms, at the lowest multipoles where the $f_{\rm NL}$ singal arises, we find differences between the migitated and true spectra of up to ∼15%, ∼25% and ∼30-35% level for the $f_{\rm NL} = -50$, 0 and 50 mocks, respectively. Nonetheless, constraining $f_{\rm NL}$ from $C_\ell^{\kappa G}$ using uncorrected maps would lead to a much larger $C_\ell^{\kappa g}$ covariance from the large amount of extra power in C_ℓ^{GG}, significantly increasing the $f_{\rm NL}$ uncertainty. For this reason, we use the mitigated maps as baseline in our cross-correlation pipeline.

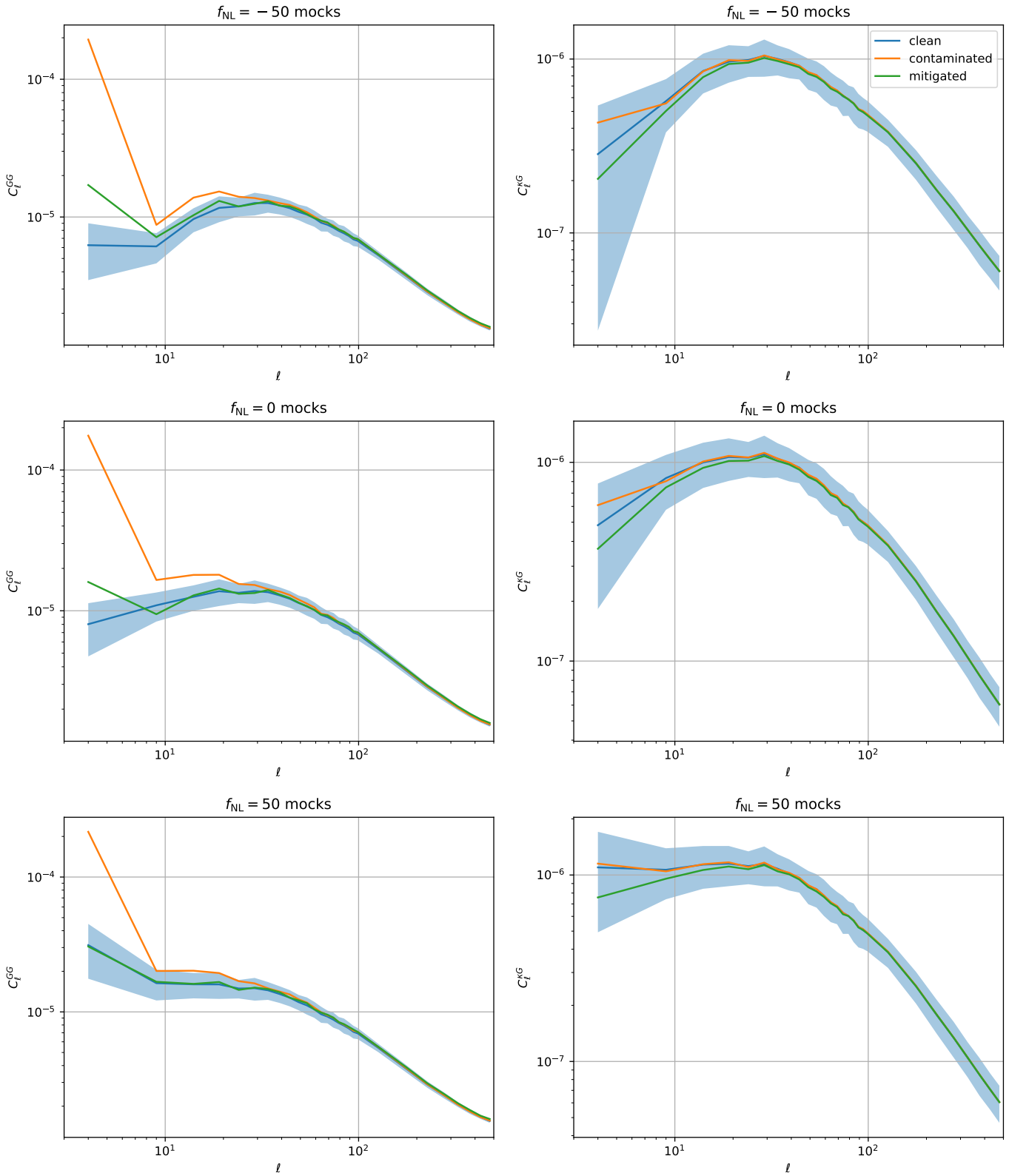

Fig. 7. Mean angular power spectra of the full sample LRG autocorrelation (left panels) and LRG-CMB lensing cross-correlation (right panels) computed from the 100 mock realizations used to test our pipeline, for various values of $f_{\rm NL}$ (-50 top panels, 0 middle panels, and 50 bottom panels). The blue lines show the true angular power spectra before adding contamination, the blue shaded area corresponds to the dispersion on the true spectra, the orange lines correspond to the angular power spectra of the contaminated mocks and the green lines to the contaminated mocks after the imaging systematics mitigation.

For C_ℓ^{GG}, the systematics mitigation presents a more complicated picture: we find that for the $f_{\rm NL} = 50$ mocks the mitigated spectra are compatible with the dispersion of the true spectra, but the performance of the mitigation pipeline depends on $f_{\rm NL}$: for

$f_{\rm NL} = -50$ and $f_{\rm NL} = 0$, the first multipole bin of the mitigated spectra is clearly still too high, lying outside the 1σ range of the clean mocks. Thus, for C_ℓ^{GG} we impose a scale cut of the first 5 multipoles contained in this bin and adopt $\ell_{\rm min} = 7$ for the parameter inference with mocks and real data. Having a larger $\ell_{\rm min}$ for C_ℓ^{GG} than for $C_\ell^{\kappa G}$ also allows us to put a joint constraint on $f_{\rm NL}$ while having a better control of systematics.

We then apply the MCMC parameter inference pipeline on the mean of the "clean" and "mitigated" angular power spectra of the 100 mock realizations for each value of $f_{\rm NL}$. We analyze $C_\ell^{\kappa G}$ and C_ℓ^{GG} separately and jointly in order to understand the impact of each observable in the constraints as well as the effects of possible remaining systematics. We list the median likelihood values with 68% confidence intervals in Tab. 1 for the mocks without systematics (clean) and in Tab. 2 for the mocks with systematics (mitigated). For the clean mocks, we find almost no intrinsic bias on the recovered $f_{\rm NL}$ values, having always a $\lesssim 0.3\sigma$ agreement with the input. For the constraints from $C_\ell^{\kappa G}$ on mocks after contamination and systematics mitigation, the input $f_{\rm NL}$ is always within the 1σ error bars of the measurements on mocks, and the bias on the measured $f_{\rm NL}$ is also lower than 0.5σ for the $f_{\rm NL} = 0$ and $f_{\rm NL} = -50$ mocks. The larger disagreement between the measured and true values for the $f_{\rm NL} = 50$ mocks can be interpreted as a consequence of an overfitted power spectrum after applying the systematics mitigation pipeline (with the bottom right panel of Fig. 7 showing the largest offset between mitigated and clean in the lowest ℓ bin, in units of the standard deviation). For C_ℓ^{GG}, we also find a level of agreement between the measured and true $f_{\rm NL}$ values within 1σ, however, in this case, the highest bias on the measurement happens for the $f_{\rm NL} = -50$ mocks. For the joint $C_\ell^{\kappa G} + C_\ell^{GG}$ tests, using $\ell_{\rm min} = 7$ for C_ℓ^{GG} we find a good agreement for the zero and positive $f_{\rm NL}$ cases, and a $\lesssim 1\sigma$ bias on the $f_{\rm NL} = -50$ mocks. Additionally, due to the systematics uncertainties on C_ℓ^{GG}, we measure the constraints from mocks using a joint approach in which we keep the C_ℓ^{GG} information for $\ell > 32$ only, in such a way that it constrains the galaxy bias but does not affect the scales where the $f_{\rm NL}$ signal arises.

The results of the tests on mocks with systematics reported in Tab. 2 are driven by the impact of the systematics mitigation on the angular power spectra shown in Fig. 7: for the negative $f_{\rm NL}$ mocks, there is a quite limited (∼15%) overfit on $C_\ell^{\kappa G}$ and some remaining power for C_ℓ^{GG} , while for positive $f_{\rm NL}$ mocks there is a stronger overfit ($\gtrsim 30\%$) on $C_\ell^{\kappa G}$ and the true power spectrum is almost perfectly recovered for C_ℓ^{GG}. In consequence, for the negative $f_{\rm NL}$ mocks, the constraints from $C_\ell^{\kappa G}$ present almost no bias with respect to the true $f_{\rm NL}$, while the constraints from C_ℓ^{GG} are biased by $\lesssim 1\sigma$ towards higher $f_{\rm NL}$ values, likely due to remaining systematics. The opposite behavior is found for the positive $f_{\rm NL}$ mocks: the constraints from $C_\ell^{\kappa G}$ are biased by $\lesssim 1\sigma$ while the constraints from C_ℓ^{GG} present a better accuracy. For the $f_{\rm NL} = 0$ mocks, we find almost no bias for C_ℓ^{GG} and a 0.5σ bias for $C_\ell^{\kappa G}$, also driven by the overfit of systematics mitigation. In the case of the joint constraints, when adopting the baseline $\ell_{\rm min} = 7$ for C_ℓ^{GG}, the constraints behave in a similar way to those from the autocorrelation, performing accurately for zero and positive $f_{\rm NL}$. Our results show that even if there could be possible biases on $f_{\rm NL}$ due to remaning or overcorrected systematics, the input $f_{\rm NL}$ is within the 1σ uncertainties of the measurement for every single case.

	$C_\ell^{\kappa G}$	C_ℓ^{GG}	$C_\ell^{\kappa G}$+C_ℓ^{GG}	$C_\ell^{\kappa G}$+C_ℓ^{GG}
Scale cut	$\ell_{\rm min} = 2$	$\ell_{\rm min} = 7$	$\ell_{\rm min} = 2, 7$	$\ell_{\rm min} = 2, 32$
$f_{\rm NL}^{\rm true} = $ -50	-50 ± 30	-43^{+22}_{-23}	-45 ± 21	-39 ± 27
$f_{\rm NL}^{\rm true} = 0$	5^{+31}_{-35}	3^{+20}_{-21}	5 ± 19	9^{+30}_{-27}
$f_{\rm NL}^{\rm true} = 50$	49^{+35}_{-34}	45^{+21}_{-20}	49^{+16}_{-17}	58^{+31}_{-32}

Table 1. Median likelihood $f_{\rm NL}$ values with 68% confidence intervals obtained from the application of our analysis pipeline to clean Gaussian mocks with $f_{\rm NL}$ = -50, 0 and 50. The constraints from C_ℓ^{GG} use a scale cut at $\ell_{\rm min} = 7$ to have a better control of systematics, while the constraints from $C_\ell^{\kappa G}$ are obtained using $\ell_{\rm min} = 2$ and $\ell_{\rm max} = 300$. The joint constraints include also a case in which the scale cut for C_ℓ^{GG} is set to $\ell_{\rm min} = 32$ in order to constrain only the galaxy bias but not $f_{\rm NL}$.

	$C_\ell^{\kappa G}$	C_ℓ^{GG}	$C_\ell^{\kappa G}$+C_ℓ^{GG}	$C_\ell^{\kappa G}$+C_ℓ^{GG}
Scale cut	$\ell_{\rm min} = 2$	$\ell_{\rm min} = 7$	$\ell_{\rm min} = 2, 7$	$\ell_{\rm min} = 2, 32$
$f_{\rm NL}^{\rm true} = $ -50	-48^{+34}_{-31}	-34^{+22}_{-27}	-30^{+19}_{-21}	-30 ± 27
$f_{\rm NL}^{\rm true} = 0$	-17^{+37}_{-35}	-4^{+24}_{-23}	-1^{+17}_{-18}	-3^{+30}_{-28}
$f_{\rm NL}^{\rm true} = 50$	21 ± 32	48^{+17}_{-19}	46^{+15}_{-16}	37 ± 28

Table 2. Median likelihood $f_{\rm NL}$ values with 68% confidence intervals obtained from the application of our analysis pipeline to contaminated and mitigated Gaussian mocks with $f_{\rm NL}$ = -50, 0 and 50. The constraints from C_ℓ^{GG} use a scale cut at $\ell_{\rm min} = 7$ to have a better control of systematics, while the constraints from $C_\ell^{\kappa G}$ are obtained using $\ell_{\rm min} = 2$ and $\ell_{\rm max} = 300$. The joint constraints include also a case in which the scale cut for C_ℓ^{GG} is set to $\ell_{\rm min} = 32$ in order to constrain only the galaxy bias but not $f_{\rm NL}$.

6. Results

We list in Tab. 3 the median likelihood values with 68% confidence intervals for $f_{\rm NL}$ and b_0, obtained from the MCMC analysis applied to $C_\ell^{\kappa G}$ and C_ℓ^{GG} separately and jointly. We obtain an uncertainty $\sigma(f_{\rm NL}) \lesssim 40$ when using the $C_\ell^{\kappa G}$ cross-correlation only. Using a scale cut at $\ell_{\rm min} = 7$, this uncertainty is reduced to $\sigma(f_{\rm NL}) \sim 25$ from C_ℓ^{GG} only and to $\sigma(f_{\rm NL}) \sim 20$ from the combination of both observables. The median likelihood values of $f_{\rm NL}$ suggest a preference of this LRG sample for positive values of $f_{\rm NL}$ which could be interpreted as a consequence of remaining systematics. However, taking into account the error bars, our results are consistent with a ΛCDM universe with Gaussian initial conditions at $\sim 1\sigma$ level for $C_\ell^{\kappa G}$ and $\gtrsim 1\sigma$ when combining this information with the LRG autospectra C_ℓ^{GG}. For the galaxy bias parameter b_0, we obtain a compatible result with previous measurements using this LRG sample, e.g. Zhou et al. (2021) measured $b_0 \sim 1.5$ assuming a redshift evolution proportional to $D(z)^{-1}$. Fig. 8 shows the 68% and 95% confidence ellipses for the $f_{\rm NL}$ - b_0 plane obtained from the two observables and their combination.

We have assumed as a baseline fiducial cosmology the $\sigma_8 \sim 0.77$ measurement from the cross-correlation between ACT lensing and this LRG sample (Sailer et al. 2024; Kim et al. 2024). As a robustness test, we recompute the constraints assuming the *Planck* 2018 bestfit value for this parameter, $\sigma_8 \sim 0.81$ (Planck Collaboration et al. 2020). We show in Fig. 9 the comparison between the $C_\ell^{\kappa G}$ constraints on the $f_{\rm NL}$ - b_0 plane assuming the baseline and the *Planck* bestfit values for σ_8. Assuming the *Planck* σ_8, we find $f_{\rm NL} = 42^{+44}_{-40}$. The median likelihood $f_{\rm NL}$ value is unaffected with respect to the $\sigma_8 = 0.77$ case listed in Tab. 3, while the 68% confidence interval is ∼10% larger. This

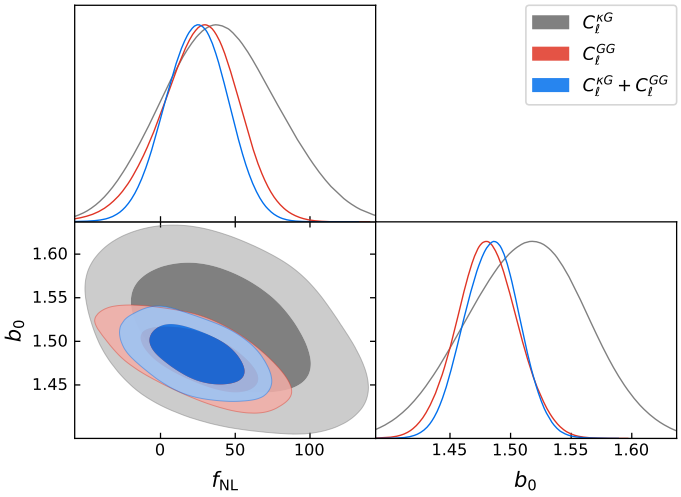

Fig. 8. 1σ and 2σ confidence ellipses for the joint posterior distribution of the $f_{\rm NL}$ and b_0 parameters obtained from the $C_\ell^{\kappa G}$ cross-correlation (grey contours), the C_ℓ^{GG} autocorrelation (red contours) and both observables jointly (blue contours).

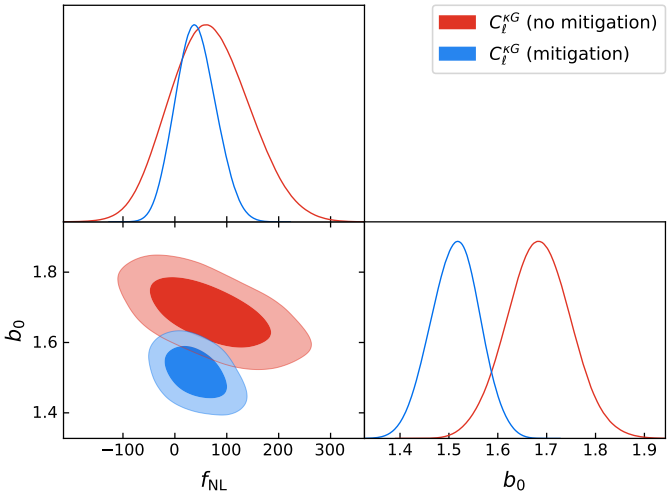

Fig. 10. 1σ and 2σ confidence ellipses for the joint posterior distribution of the $f_{\rm NL}$ and b_0 parameters obtained from the $C_\ell^{\kappa G}$ cross-correlation. The blue contours correspond to the baseline constraints after applying the SYSnet mitigation weights to the data and the red contours to the case in which no systematics mitigation is performed.

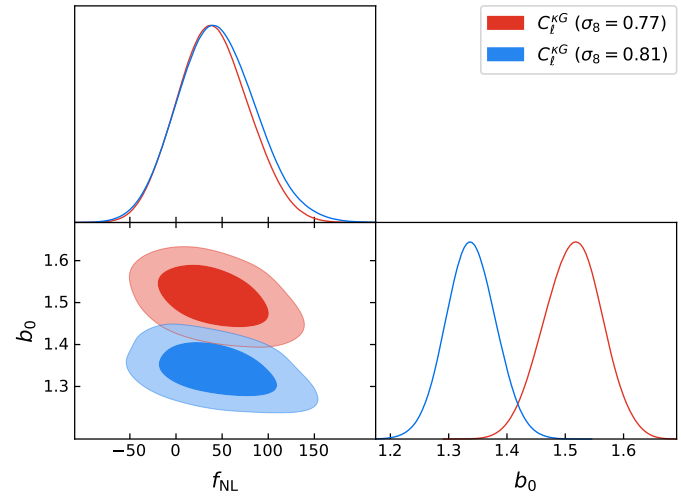

Fig. 9. 1σ and 2σ confidence ellipses for the joint posterior distribution of the $f_{\rm NL}$ and b_0 parameters obtained from the $C_\ell^{\kappa G}$ cross-correlation. The blue contours assume a fiducial cosmology with the *Planck* σ_8 while the red contours assume the σ_8 preferred by the LRG sample analyzed in this paper.

	$C_\ell^{\kappa G}$	C_ℓ^{GG}	$C_\ell^{\kappa G}$+C_ℓ^{GG}	$C_\ell^{\kappa G}$+C_ℓ^{GG}
Scale cut	$\ell_{\rm min} = 2$	$\ell_{\rm min} = 7$	$\ell_{\rm min} = 2, 7$	$\ell_{\rm min} = 2, 32$
$f_{\rm NL}$	39^{+40}_{-38}	27^{+24}_{-28}	24^{+20}_{-21}	45^{+38}_{-36}
b_0	$1.51^{+0.05}_{-0.05}$	$1.48^{+0.02}_{-0.02}$	$1.48^{+0.02}_{-0.02}$	$1.48^{+0.03}_{-0.02}$

Table 3. Median likelihood $f_{\rm NL}$ and b_0 values with 68% confidence intervals obtained from the application of our analysis pipeline to the LRG data and their cross-correlation with the *Planck* CMB lensing. The constraints from C_ℓ^{GG} use a scale cut at $\ell_{\rm min} = 7$ to have a better control of systematics, while the constraints from $C_\ell^{\kappa G}$ are obtained using all the multipoles up to $\ell_{\rm max} = 300$. The joint constraints include also a case in which the scale cut for C_ℓ^{GG} is set to $\ell_{\rm min} = 32$ in order to constrain only the galaxy bias but not $f_{\rm NL}$.

Region	$C_\ell^{\kappa G}(\ell_{\rm min} = 2)$	$C_\ell^{GG}(\ell_{\rm min} = 7)$	$C_\ell^{\kappa G}$+C_ℓ^{GG}
NGC	90^{+208}_{-174}	30 ± 43	20 ± 40
SGC	82^{+118}_{-112}	26^{+28}_{-31}	36^{+26}_{-29}

Table 4. Consistency check for the median likelihood $f_{\rm NL}$ values with 68% confidence intervals obtained from the application of our analysis pipeline to the different sky regions (NGC and SGC) of the LRG data and their cross-correlation with the *Planck* CMB lensing.

larger uncertainty is essentially due to a lower b_0 value measured as a consequence of assuming a larger σ_8, which affects the amplitude of the $(b - p)$ term that enhances the $f_{\rm NL}$ signal (see Eq. 2).

In order to understand the stability of our $f_{\rm NL}$ measurement from $C_\ell^{\kappa G}$ in terms of systematics, we compare in Fig. 10 the constraints from the *Planck* lensing - DESI LRG cross-correlation with the case in which no systematics mitigation is performed. In the latter case, we find $f_{\rm NL} = 64^{+80}_{-73}$. The result is compatible with the baseline case using systematics weights, but the uncertainties are larger due to the impact of the extra C_ℓ^{GG} power spectrum in the covariance matrix. This also emphasizes the importance of performing an accurate systematics mitigation even for cross-correlation analysis.

We also test the robustness of our results to the systematics looking at the stability of the results as a function of the minimum multipole $\ell_{\rm min}$. In Fig. 11 we represent the constraints on $f_{\rm NL}$ from $C_\ell^{\kappa G}$ and C_ℓ^{GG} for $\ell_{\rm min} = 2$, 7 and 12. For $C_\ell^{\kappa G}$, the constraints are compatible at $\lesssim 1\sigma$ level with $f_{\rm NL} = 0$ for the three $\ell_{\rm min}$ values. Instead for C_ℓ^{GG}, we find a $\sim 1\sigma$ deviation for $\ell_{\rm min} = 7$, while this deviation grows up to $\sim 2\sigma$ for $\ell_{\rm min} = 2$ and $\ell_{\rm min} = 12$. This indicates the lower multipoles on C_ℓ^{GG} might be dominated by observational systematics, as suggested from the test on mocks, while for $C_\ell^{\kappa G}$ it is safer to include all the scales in the analysis.

In addition, we test the compatibility of our results among different regions on the sky. We compute our constraints on $f_{\rm NL}$ by applying masks of the North and South galactic caps (NGC and SGC) and list the results in Tab. 4. We find compatible results between the two galactic caps, and even if the bestfit $f_{\rm NL}$ values obtaiined from $C_\ell^{\kappa G}$ are consistently higher for than those

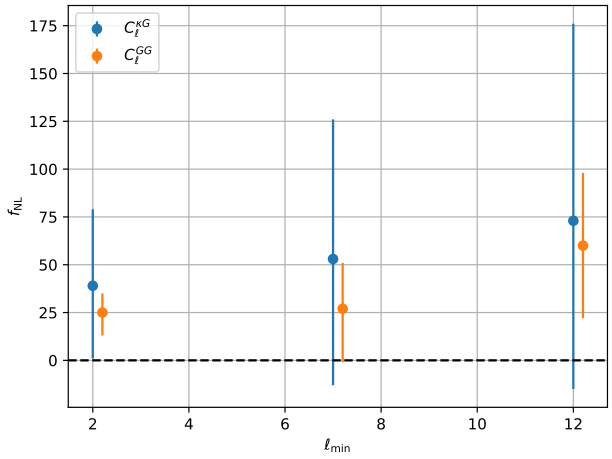

Fig. 11. Constraints on $f_{\rm NL}$ from $C_\ell^{\kappa G}$ (orange dots) and C_ℓ^{GG} (blue dots) with 68% confidence interval as a function of the minimum multipole $\ell_{\rm min}$ included in the analysis.

measured from the full footprint, the measurements are compatible with zero PNG considering the larger error bars.

Our constraint on $f_{\rm NL}$ from the DESI LRG - *Planck* lensing cross-correlation is also compatible with the main result from Rezaie et al. (2023) using the LRG autocorrelation only. Rezaie et al. (2023) discussed in detail the impact of the mitigation recipe on the $f_{\rm NL}$ error bars and best-fit values. They highlighted $f_{\rm NL} = 34^{+24}_{-44}$ when applying a more aggressive nonlinear regression for systematics mitigation using 9 features maps, while we have selected here a more conservative treatment in order to avoid a strong overfit in the cross-correlation $C_\ell^{\kappa G}$. When applying the same nonlinear treatment with 3 maps than we choose for this study, they find $f_{\rm NL} = 28^{+12}_{-11}$ (before calibration) and $f_{\rm NL} = 47 \pm 14$ (after calibration). Note that in Rezaie et al. (2023) a calibration of the constraints was proposed based on the results of the tests on mocks, and that all multipoles were included in the baseline analysis, while we have not applied any calibration and we have set $\ell_{\rm min} = 7$ for C_ℓ^{GG}. Another important difference in the analysis is the contamination model on the mocks: we have used nonlinear weights for implementing the contamination on the mocks, while in Rezaie et al. (2023) linear weights were applied to generate this contamination. A calibration of the $f_{\rm NL}$ constraints based on the mocks would be model dependent in any case, and our aim is instead to show the capabilities of $C_\ell^{\kappa G}$ to produce more stable measurements on $f_{\rm NL}$, either alone or in combination with C_ℓ^{GG}.

7. Conclusions

In this work, we have used an LRG catalog from the DESI Legacy imaging surveys calibrated with the spectroscopic redshifts that have been observed for the DESI Survey Validation, in combination with the *Planck* PR4 CMB lensing map, to put a constraint on the primordial local non-Gaussianity parameter $f_{\rm NL}$. We have measured $f_{\rm NL}$ through the scale-dependent bias effect using as observables the cross-correlation between the LRG and CMB lensing maps in the angular domain, $C_\ell^{\kappa G}$, and the autocorrelation of the LRG field C_ℓ^{GG}.

In order to limit the impact of imaging systematics on large scales where the $f_{\rm NL}$ signal is present, we have used a neural network code for imaging systematics mitigation. Our measurement is performed without blinding, but the full analysis methodology is tested on mock fields including imaging systematics for different $f_{\rm NL}$ values. Our end-to-end pipeline works at a reasonable level of agreement with the input $f_{\rm NL}$ values, being especially robust when combining both $C_\ell^{\kappa G}$ and C_ℓ^{GG} for the positive and zero $f_{\rm NL}$ mocks. From the systematics tests on mocks, we find residual contamination in the behavior of the 5 first multipoles ($\ell = 2-6$) of C_ℓ^{GG}; hence, we impose a cut at $\ell_{\rm min} = 7$ for the autocorrelation power spectrum.

Just from the CMB - LRG cross-correlation $C_\ell^{\kappa G}$, we find $f_{\rm NL} = 39^{+40}_{-38}$ at 68% confidence level. We perform some robustness tests on this result such as changing the fiducial σ_8 to the *Planck* best-fit instead of the LRG catalog best-fit or varying the minimum multipole $\ell_{\rm min}$ to evaluate the possible impact of systematics and find consistent results. If we combine our result with the information from the angular LRG autocorrelation C_ℓ^{GG} adopting the $\ell_{\rm min} = 7$ cut, we find $f_{\rm NL} = 24^{+20}_{-21}$, although C_ℓ^{GG} presents a larger statistical fluctuation as a function of $\ell_{\rm min}$, suggesting that $C_\ell^{\kappa G}$ is more stable and less sensitive to the effect of imaging systematics. Our results are consistent with the $f_{\rm NL}$ measurements from the DESI LRG by Rezaie et al. (2023) and motivate the use of CMB cross-correlation for measuring $f_{\rm NL}$ with further catalogs as a technique to limit the impact of imaging systematics.

Data availability

All data points, maps, covariances and MCMC chains shown in the figures of this paper are publicly available in `https://doi.org/10.5281/zenodo.14401463`.

Acknowledgements. J. R. Bermejo-Climent and R. Demina acknowledge support from the U.S. Department of Energy under the grant DE-SC0008475.0. JRBC acknowledges the support of the Spanish Ministry of Science and Innovation project PID2021-126616NB-I00. AK was supported as a CITA National Fellow by the Natural Sciences and Engineering Research Council of Canada (NSERC), funding reference #DIS-2022-568580. MR is supported by the U.S. Department of Energy grants DE-SC0021165 and DE-SC0011840. This material is based upon work supported by the U.S. Department of Energy (DOE), Office of Science, Office of High-Energy Physics, under Contract No. DE–AC02–05CH11231, and by the National Energy Research Scientific Computing Center, a DOE Office of Science User Facility under the same contract. Additional support for DESI was provided by the U.S. National Science Foundation (NSF), Division of Astronomical Sciences under Contract No. AST-0950945 to the NSF's National Optical-Infrared Astronomy Research Laboratory; the Science and Technology Facilities Council of the United Kingdom; the Gordon and Betty Moore Foundation; the Heising-Simons Foundation; the French Alternative Energies and Atomic Energy Commission (CEA); the National Council of Humanities, Science and Technology of Mexico (CONAHCYT); the Ministry of Science, Innovation and Universities of Spain (MICIU/AEI/10.13039/501100011033), and by the DESI Member Institutions: `https://www.desi.lbl.gov/collaborating-institutions`. The DESI Legacy Imaging Surveys consist of three individual and complementary projects: the Dark Energy Camera Legacy Survey (DECaLS), the Beijing-Arizona Sky Survey (BASS), and the Mayall z-band Legacy Survey (MzLS). DECaLS, BASS and MzLS together include data obtained, respectively, at the Blanco telescope, Cerro Tololo Inter-American Observatory, NSF's NOIRLab; the Bok telescope, Steward Observatory, University of Arizona; and the Mayall telescope, Kitt Peak National Observatory, NOIRLab. NOIRLab is operated by the Association of Universities for Research in Astronomy (AURA) under a cooperative agreement with the National Science Foundation. Pipeline processing and analyses of the data were supported by NOIRLab and the Lawrence Berkeley National Laboratory. Legacy Surveys also uses data products from the Near-Earth Object Wide-field Infrared Survey Explorer (NEOWISE), a project of the Jet Propulsion Laboratory/California Institute of Technology, funded by the National Aeronautics and Space Administration. Legacy Surveys was supported by: the Director, Office of Science, Office of High Energy Physics of the U.S. Department of Energy; the National Energy Research Scientific Computing Center, a DOE Office of Science User Facility; the U.S. National Science Foundation, Division of Astronomical Sciences; the National Astronomical Observatories of China, the Chinese Academy of Sciences and the Chinese National Natural Science Foun-

dation. LBNL is managed by the Regents of the University of California under contract to the U.S. Department of Energy. The complete acknowledgments can be found at https://www.legacysurvey.org/. Any opinions, findings, and conclusions or recommendations expressed in this material are those of the author(s) and do not necessarily reflect the views of the U. S. National Science Foundation, the U. S. Department of Energy, or any of the listed funding agencies. The authors are honored to be permitted to conduct scientific research on Iolkam Du'ag (Kitt Peak), a mountain with particular significance to the Tohono O'odham Nation.

References

Adame, A. G., Avila, S., Gonzalez-Perez, V., et al. 2024, Astron. Astrophys., 689, A69
Afshordi, N. & Tolley, A. J. 2008, Physical Review D, 78
Akrami, Y., Andersen, K. J., Ashdown, M., et al. 2020, Astron. Astrophys., 643, A42
Alonso, D., Sanchez, J., & Slosar, A. 2019, Mon. Not. Roy. Astron. Soc., 484, 4127
Ballardini, M., Matthewson, W. L., & Maartens, R. 2019, Monthly Notices of the Royal Astronomical Society, 489, 1950–1956
Bardeen, J. M., Steinhardt, P. J., & Turner, M. S. 1983, Phys. Rev. D, 28, 679
Barreira, A. 2020, Journal of Cosmology and Astroparticle Physics, 2020, 031–031
Barreira, A. 2022, Journal of Cosmology and Astroparticle Physics, 2022, 013
Bermejo-Climent, J. R., Ballardini, M., Finelli, F., et al. 2021, Physical Review D, 103
Cabass, G., Ivanov, M. M., Philcox, O. H. E., Simonović, M., & Zaldarriaga, M. 2022, Phys. Rev. D, 106, 043506
Cagliari, M. S., Castorina, E., Bonici, M., & Bianchi, D. 2023, Optimal constraints on Primordial non-Gaussianity with the eBOSS DR16 quasars in Fourier space
Carbone, C., Verde, L., & Matarrese, S. 2008, The Astrophysical Journal, 684, L1–L4
Carron, J., Mirmelstein, M., & Lewis, A. 2022, Journal of Cosmology and Astroparticle Physics, 2022, 039
Castorina, E., Hand, N., Seljak, U., et al. 2019, Journal of Cosmology and Astroparticle Physics, 2019, 010–010
Chaussidon, E., Yèche, C., de Mattia, A., et al. 2024, Constraining primordial non-Gaussianity with DESI 2024 LRG and QSO samples
Chaussidon, E., Yèche, C., Palanque-Delabrouille, N., et al. 2021, Monthly Notices of the Royal Astronomical Society, 509, 3904
Chen, X. 2010, Advances in Astronomy, 2010
Dalal, N., Doré, O., Huterer, D., & Shirokov, A. 2008, Phys. Rev. D, 77, 123514
D'Amico, G., Lewandowski, M., Senatore, L., & Zhang, P. 2023, Limits on primordial non-Gaussianities from BOSS galaxy-clustering data
DESI Collaboration, Abareshi, B., Aguilar, J., et al. 2022, AJ, 164, 207
DESI Collaboration, Adame, A. G., Aguilar, J., et al. 2023, arXiv e-prints, arXiv:2306.06308
DESI Collaboration, Adame, A. G., Aguilar, J., et al. 2024a, AJ, 167, 62
DESI Collaboration, Adame, A. G., Aguilar, J., et al. 2024b, arXiv e-prints, arXiv:2404.03002
DESI Collaboration, Adame, A. G., Aguilar, J., et al. 2024c, arXiv e-prints, arXiv:2404.03001
DESI Collaboration, Adame, A. G., Aguilar, J., et al. 2024d, arXiv e-prints, arXiv:2404.03000
DESI Collaboration, Adame, A. G., Aguilar, J., et al. 2024e, DESI 2024 V: Full-Shape Galaxy Clustering from Galaxies and Quasars
DESI Collaboration, Adame, A. G., Aguilar, J., et al. 2024f, DESI 2024 VII: Cosmological Constraints from the Full-Shape Modeling of Clustering Measurements
DESI Collaboration, Aghamousa, A., Aguilar, J., et al. 2016a, arXiv e-prints, arXiv:1611.00037
DESI Collaboration, Aghamousa, A., Aguilar, J., et al. 2016b, arXiv e-prints, arXiv:1611.00036
Dey, A. et al. 2019, Astron. J., 157, 168
Flaugher, B., Diehl, H. T., Honscheid, K., et al. 2015, AJ, 150, 150
Foreman-Mackey, D., Hogg, D. W., Lang, D., & Goodman, J. 2013, Publications of the Astronomical Society of the Pacific, 125, 306–312
García-García, C., Alonso, D., & Bellini, E. 2019, J. Cosmology Astropart. Phys., 2019, 043
Giannantonio, T., Scranton, R., Crittenden, R. G., et al. 2008, Physical Review D, 77
Giusarma, E., Vagnozzi, S., Ho, S., et al. 2018, Physical Review D, 98
Gorski, K. M., Hivon, E., Banday, A. J., et al. 2005, The Astrophysical Journal, 622, 759–771
Grossi, M., Verde, L., Carbone, C., et al. 2009, Monthly Notices of the Royal Astronomical Society, 398, 321–332
Guth, A. H. 1981, Phys. Rev. D, 23, 347
Guth, A. H. & Pi, S.-Y. 1985, Phys. Rev. D, 32, 1899
Guy, J., Bailey, S., Kremin, A., et al. 2023, AJ, 165, 144
Hivon, E., Gorski, K. M., Netterfield, C. B., et al. 2002, The Astrophysical Journal, 567, 2–17
Hu, W. & Okamoto, T. 2002, The Astrophysical Journal, 574, 566–574
Kim, J., Sailer, N., Madhavacheril, M. S., et al. 2024, The Atacama Cosmology Telescope DR6 and DESI: Structure formation over cosmic time with a measurement of the cross-correlation of CMB Lensing and Luminous Red Galaxies
Kitanidis, E. & White, M. 2021, Mon. Not. Roy. Astron. Soc., 501, 6181
Komatsu, E. & Spergel, D. N. 2001, Phys. Rev. D, 63, 063002
Krolewski, A., Percival, W. J., Ferraro, S., et al. 2024, Journal of Cosmology and Astroparticle Physics, 2024, 021
Langlois, D. 2010, Inflation and Cosmological Perturbations (Springer Berlin Heidelberg), 1–57
Levi, M., Bebek, C., Beers, T., et al. 2013, arXiv e-prints, arXiv:1308.0847
Lewis, A. & Challinor, A. 2011, CAMB: Code for Anisotropies in the Microwave Background, Astrophysics Source Code Library, record ascl:1102.026
Miller, T. N., Doel, P., Gutierrez, G., et al. 2024, AJ, 168, 95
Mueller, E.-M., Rezaie, M., Percival, W. J., et al. 2021, arXiv e-prints, arXiv:2106.13725
Planck Collaboration et al. 2019, Planck 2018 results. IX. Constraints on primordial non-Gaussianity
Planck Collaboration et al. 2020, Astron. Astrophys., 641, A6, [Erratum: Astron.Astrophys. 652, C4 (2021)]
Rezaie, M., Ross, A. J., Seo, H.-J., et al. 2023, Local primordial non-Gaussianity from the large-scale clustering of photometric DESI luminous red galaxies
Rezaie, M., Seo, H.-J., Ross, A. J., & Bunescu, R. C. 2020, MNRAS, 495, 1613
Ross, A. J., Percival, W. J., Carnero, A., et al. 2012, Monthly Notices of the Royal Astronomical Society, 428, 1116–1127
Sailer, N., Kim, J., Ferraro, S., et al. 2024, Cosmological constraints from the cross-correlation of DESI Luminous Red Galaxies with CMB lensing from Planck PR4 and ACT DR6
Schlafly, E. F., Kirkby, D., Schlegel, D. J., et al. 2023, AJ, 166, 259
Schmittfull, M. & Seljak, U. 2018, Physical Review D, 97
Serra, P., Lagache, G., Doré, O., Pullen, A., & White, M. 2014, Astron. Astrophys., 570, A98
Silber, J. H., Fagrelius, P., Fanning, K., et al. 2023, AJ, 165, 9
Slosar, A., Hirata, C., Seljak, U., Ho, S., & Padmanabhan, N. 2008, Journal of Cosmology and Astroparticle Physics, 2008, 031
Smith, K. M., Zahn, O., & Doré, O. 2007, Physical Review D, 76
Starobinsky, A. 1980, Physics Letters B, 91, 99
Starobinsky, A. 1982, Physics Letters B, 117, 175
Takahashi, R., Sato, M., Nishimichi, T., Taruya, A., & Oguri, M. 2012, The Astrophysical Journal, 761, 152
Takahashi, T. 2014, Progress of Theoretical and Experimental Physics, 2014, 06B105
Vazquez Gonzalez, J. A., Padilla, L. E., & Matos, T. 2020, Revista Mexicana de Física E, 17, 73–91
White, M., Zhou, R., DeRose, J., et al. 2022a, Journal of Cosmology and Astroparticle Physics, 2022, 007
White, M. et al. 2022b, JCAP, 02, 007
Zhou, R., Dey, B., Newman, J. A., et al. 2023a, The Astronomical Journal, 165, 58
Zhou, R., Ferraro, S., White, M., et al. 2023b, Journal of Cosmology and Astroparticle Physics, 2023, 097
Zhou, R. et al. 2021, Mon. Not. Roy. Astron. Soc., 501, 3309
Zou, H., Zhou, X., Fan, X., et al. 2017, Publications of the Astronomical Society of the Pacific, 129, 064101

[1] Department of Physics & Astronomy, University of Rochester, 206 Bausch and Lomb Hall, P.O. Box 270171, Rochester, NY 14627-0171, USA
[2] Instituto de Astrofísica de Canarias, C/ Vía Láctea, s/n, E-38205 La Laguna, Tenerife, Spain
[3] Department of Physics and Astronomy, University of Waterloo, 200 University Ave W, Waterloo, ON N2L 3G1, Canada
[4] Perimeter Institute for Theoretical Physics, 31 Caroline St. North, Waterloo, ON N2L 2Y5, Canada
[5] Waterloo Centre for Astrophysics, University of Waterloo, 200 University Ave W, Waterloo, ON N2L 3G1, Canada
[6] Lawrence Berkeley National Laboratory, 1 Cyclotron Road, Berkeley, CA 94720, USA

[7] Department of Physics, Kansas State University, 116 Cardwell Hall, Manhattan, KS 66506, USA
[8] Physics Dept., Boston University, 590 Commonwealth Avenue, Boston, MA 02215, USA
[9] Dipartimento di Fisica "Aldo Pontremoli", Università degli Studi di Milano, Via Celoria 16, I-20133 Milano, Italy
[10] Department of Physics & Astronomy, University College London, Gower Street, London, WC1E 6BT, UK
[11] IRFU, CEA, Université Paris-Saclay, F-91191 Gif-sur-Yvette, France
[12] Instituto de Física, Universidad Nacional Autónoma de México, Circuito de la Investigación Científica, Ciudad Universitaria, Cd. de México C. P. 04510, México
[13] NSF NOIRLab, 950 N. Cherry Ave., Tucson, AZ 85719, USA
[14] University of California, Berkeley, 110 Sproul Hall #5800 Berkeley, CA 94720, USA
[15] Departamento de Física, Universidad de los Andes, Cra. 1 No. 18A-10, Edificio Ip, CP 111711, Bogotá, Colombia
[16] Observatorio Astronómico, Universidad de los Andes, Cra. 1 No. 18A-10, Edificio H, CP 111711 Bogotá, Colombia
[17] Institut d'Estudis Espacials de Catalunya (IEEC), c/ Esteve Terradas 1, Edifici RDIT, Campus PMT-UPC, 08860 Castelldefels, Spain
[18] Institute of Cosmology and Gravitation, University of Portsmouth, Dennis Sciama Building, Portsmouth, PO1 3FX, UK
[19] Institute of Space Sciences, ICE-CSIC, Campus UAB, Carrer de Can Magrans s/n, 08913 Bellaterra, Barcelona, Spain
[20] Fermi National Accelerator Laboratory, PO Box 500, Batavia, IL 60510, USA
[21] Department of Astrophysical Sciences, Princeton University, Princeton NJ 08544, USA
[22] Center for Cosmology and AstroParticle Physics, The Ohio State University, 191 West Woodruff Avenue, Columbus, OH 43210, USA
[23] Department of Physics, The Ohio State University, 191 West Woodruff Avenue, Columbus, OH 43210, USA
[24] The Ohio State University, Columbus, 43210 OH, USA
[25] School of Mathematics and Physics, University of Queensland, Brisbane, QLD 4072, Australia
[26] Department of Physics, Southern Methodist University, 3215 Daniel Avenue, Dallas, TX 75275, USA
[27] Department of Physics and Astronomy, University of California, Irvine, 92697, USA
[28] Sorbonne Université, CNRS/IN2P3, Laboratoire de Physique Nucléaire et de Hautes Energies (LPNHE), FR-75005 Paris, France
[29] Departament de Física, Serra Húnter, Universitat Autònoma de Barcelona, 08193 Bellaterra (Barcelona), Spain
[30] Institut de Física d'Altes Energies (IFAE), The Barcelona Institute of Science and Technology, Edifici Cn, Campus UAB, 08193, Bellaterra (Barcelona), Spain
[31] Institució Catalana de Recerca i Estudis Avançats, Passeig de Lluís Companys, 23, 08010 Barcelona, Spain
[32] Department of Physics and Astronomy, Siena College, 515 Loudon Road, Loudonville, NY 12211, USA
[33] Department of Physics & Astronomy and Pittsburgh Particle Physics, Astrophysics, and Cosmology Center (PITT PACC), University of Pittsburgh, 3941 O'Hara Street, Pittsburgh, PA 15260, USA
[34] Departamento de Física, DCI-Campus León, Universidad de Guanajuato, Loma del Bosque 103, León, Guanajuato C. P. 37150, México.
[35] Instituto Avanzado de Cosmología A. C., San Marcos 11 - Atenas 202. Magdalena Contreras. Ciudad de México C. P. 10720, México
[36] Instituto de Astrofísica de Andalucía (CSIC), Glorieta de la Astronomía, s/n, E-18008 Granada, Spain
[37] Departament de Física, EEBE, Universitat Politècnica de Catalunya, c/Eduard Maristany 10, 08930 Barcelona, Spain
[38] Physics Department, Yale University, P.O. Box 208120, New Haven, CT 06511, USA
[39] Department of Astronomy, The Ohio State University, 4055 McPherson Laboratory, 140 W 18th Avenue, Columbus, OH 43210, USA
[40] Department of Physics and Astronomy, Sejong University, 209 Neungdong-ro, Gwangjin-gu, Seoul 05006, Republic of Korea
[41] CIEMAT, Avenida Complutense 40, E-28040 Madrid, Spain
[42] University of Michigan, 500 S. State Street, Ann Arbor, MI 48109, USA
[43] Department of Physics, University of California, Berkeley, 366 LeConte Hall MC 7300, Berkeley, CA 94720-7300, USA